FOREX Publication
Open Access | Rapid and quality publishing

International Journal of
Electrical and Electronics Research (IJEER)
Research Article | Volume 14, Issue 2 | Pages 309-319 | e-ISSN: 2347-470X

Active and Reactive Power Control of DFIG for Wind Energy Generation using MRAC

Sanjit Brahma[1*] , and Ranjay Das[2]

[1]*Department of Electrical Engineering, Central Institute of Technology Kokrajhar, Assam, India; Email: ph19ee1902@cit.ac.in*
[2]*Department of Electrical Engineering, Central Institute of Technology Kokrajhar, Assam, India; Email: r.das@cit.ac.in*

***Correspondence:** *Sanjit Brahma, ph19ee1902@cit.ac.in*

ABSTRACT- The Doubly Fed Induction Generator (DFIG) utilized in wind energy conversion systems (WECS) requires regulation of both active and reactive power to ensure stability and proper functioning. Model Reference Adaptive Control (MRAC) scheme augmented with flux-oriented vector control strategy is proposed for ensuring effective power management without extra sensors. RSC (machine side converter) and GSC (grid side converter) are to be controlled using Lyapunov-based adaptive control for improved power extraction and stability of the grid. Proposed model was simulated in MATLAB/Simulink and tested under dynamic conditions of wind, including gust and ramp variation. Results show that both GSC and RSC axis current components tracks the references. MRAC-based controller has maintained the dc link stability with less than 5% overshoot. The simulation verification indicated an excellent achievement of decoupled control of power. This demonstrates MRAC's robustness for power regulation in DFIG-based WECS, which enhances reliability and stability in energy generation.

Keywords: Doubly Fed Induction Generator, Flux-Oriented Control, MPPT (Maximum Power Point Tracking), Wind Energy Conversion System, MRAC (Model Reference Adaptive Control).

ARTICLE INFORMATION

Author(s): Sanjit Brahma, and Ranjay Das
Received: 13/11/25; **Accepted**: 09/03/26; **Published**: 20/06/26;
E- ISSN: 2347-470X;
Paper Id: IJEER 1311A11;
Citation: 10.37391/ijeer.140207
Webpage-link:
https://ijeer.forexjournal.co.in/archive/volume-14/ijeer-140207.html

Publisher's Note: FOREX Publication stays neutral with regard to jurisdictional claims in Published maps and institutional affiliations.

1. INTRODUCTION

Due to a number of benefits over fixed speed technologies, such as increased power, decreased strains on the turbine, improved power quality, and acoustic noise reduction, variable-speed wind turbines have been used more frequently recently [1]. Double-fed Induction Generators (DFIGs) have become the main generator in high-power wind energy conversion systems. Power regulation is independent for both reactive and active components in the durable, low-maintenance. Voltage source converters are linked to both sides of the machine. The rotor side converter has been designed to handle a small portion, specifically 25% to 30%, of the machine's nominal power as shown in *figure 1*. This design choice helps to lower converter expenses and minimize power loss, in contrast to other systems that use fully sized converters [1]. Additionally, DFIG is a suitable choice for low- speed applications.

Stator flux orientation constitutes one of the most recognized applications among various techniques available for controlling the DFIG [2, 3]. Other techniques including direct power [4], direct torque control [5], and stator voltage orientation are also being researched and applied in the industrial sector. Regardless of the approach used, the system's ability to function depends on knowing the rotor's mechanical location, which can be obtained *via* a location encoder or a sensorless estimation technique is depicted in *figure 2*.

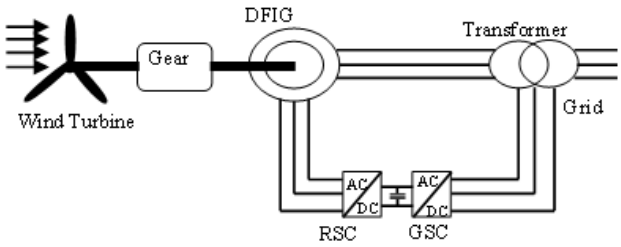

Figure 1. DFIG based WECS design

The converter's ideal switching state in [7] is determined by directly controlling the active and reactive voltages. Using a sensorless control that can start instantly, the DPC for DFIG is created in [8]. Another study, as described in reference [9], focuses on sector selection based solely on the estimated stator flux. Predictive control simplifies the analysis of harmonic filter and power converter, which has recently been used to eliminate some of the disadvantages of classical DPC, such as variable at steady-state power ripples and frequency switching [10]. It is also capable of functioning at low, steady switching frequencies. In recent years, a number of studies [11, 12] have been published that use vector control and fuzzy logic to directly regulate the DFIG with constant switching frequency while eliminating torque or power ripples [13, 14]. In [15] and [16], the authors design a small signal model of DFIG for implementation of MRAS observer with magnetizing current supplied exclusively by rotor. This technique however is not suitable for sensorless technique because the MRAS observer depends on DFIG stator current [17]. The author suggested in

FOREX Publication
Open Access | Rapid and quality publishing
International Journal of Electrical and Electronics Research (IJEER)
Research Article | Volume 14, Issue 2 | Pages 309-319 | e-ISSN: 2347-470X

[18] using basic machine voltage and current formulae to estimate rotor position. Authors designed a vector-oriented control for DFIG using MRAC combined with PI controllers in the control loop of DC-voltage as well as rotor speed. [20] Describes the design of a robust MRAC for the DFIG, implemented using a fractional-order integrator.

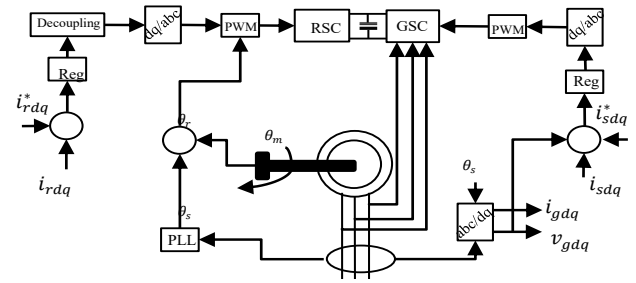

Figure 2. Schematic diagram of DFIG converters with PLL for rotor position estimation

There are two distinct components to the DFIG's MRAC controller. First, the GSC and RSC converters are described in terms of rotating reference frame. Second, the control loops for GSC and RSC are designed using the MRAC method. The GSC converter will also regulate the DC-link voltage. Despite system interruptions, such as fluctuations in wind speed, the DFIG system can be controlled in the desired manner. To verify the suggested MRAC for DFIGs, MATLAB simulation is performed to illustrate the effectiveness of the MRAC model.

Although MRAC-based DFIG control has been reported in previous studies, most works focus on rotor current regulation or speed control and often rely on hybrid PI-MRAC structures or observer-based schemes. Limited studies address coordinated adaptive control of both RSC and GSC with explicit Lyapunov stability proof under grid disturbances. Furthermore, comparative performance analysis with disturbance scenarios and implementation considerations remains insufficient in existing literature. This gap motivates the present work.

Unlike earlier MRAC-based DFIG studies that focus primarily on rotor-side control or speed regulation, the present work develops a unified Lyapunov-based MRAC framework for both grid-side and rotor-side converters within a stator-flux-oriented architecture. The controller is designed to regulate active power, reactive power, and DC-link voltage simultaneously under parameter uncertainties and grid disturbances. In addition to standard wind variations, the system is evaluated under grid voltage sag, inductance mismatch, and short-circuit disturbances. This combined stability-verified dual-converter MRAC structure and disturbance-oriented evaluation distinguishes the present study from conventional MRAC-DFIG implementations.

The main contributions of this paper are as follows:
(1) Development of a Lyapunov-based MRAC scheme for coordinated control of both rotor-side and grid-side converters.
(2) Integration of MRAC with stator-flux-oriented vector control for simultaneous active power, reactive power, and DC-link regulation.
(3) Robustness evaluation under wind variation, grid voltage sag, parameter mismatch, and short-circuit disturbances.
(4) Quantitative comparison with conventional PI control using multiple performance indices.
(5) Discussion of implementation feasibility on DSP/FPGA platforms.

2. SYSTEM MODELING FOR WIND POWER GENERATION

2.1.Modeling of Wind Turbine

Therefore, torque produced by the turbine changes with wind speeds since, wind speed and air density affect kinetic energy. The turbine power P_t and torque T_t are given as[21]:

$$\begin{cases} P_t = \frac{1}{2}\rho\pi R_w^2 V_\omega^3 C_p(\lambda,\beta) \\ T_t = \frac{1}{2}\rho\pi R_w^2 V_\omega^3 \frac{C_p(\lambda,\beta)}{\omega_t} \end{cases} \quad (1)$$

Power coefficient as [22]:

$$C_p(\lambda,\beta) = C_1\left(\frac{C_2}{\lambda_i} - C_3\beta - C_4\right)e^{-\frac{12.5}{\lambda_i}} + C_6\lambda \quad (2)$$

Where, λ as the tip speed ratio (TSR) while β as blade angle of pitch , as given below:

$$\lambda = \frac{\omega_t R_w}{V_\omega} \quad (3)$$

The camshaft must always be adjusted to ramp within a very narrow band, which is achieved only by putting the camshaft in a set against the drive shaft by means of some gearbox. The generator rotor shaft speed ω_m and mechanical torque T_m, which are provided in the gearbox's generator side, are as follows, disregarding the losses in the transmission:

$$T_m = \frac{T_t}{N} \;\; and \;\; \omega_m = \frac{\omega_t}{N} \quad (4)$$

Where, *N* denotes the gearbox ratio.

2.2.Maximum Power Point Tracking

The Betz limit defines the theoretical maximum efficiency of a wind turbine at approximately 59.3%, corresponding to a power coefficient of $C_{p-opt} = 0.441198$ [23]. This optimal point is achieved at a blade pitch angle $\beta = 0$ and top speed ratio $\lambda_{p-opt} = 7.2$, representing the Maximum Power Point Tracking (MPPT) condition. *Figure 3* shows the curve for the power coefficient and the speed ratio of tip.

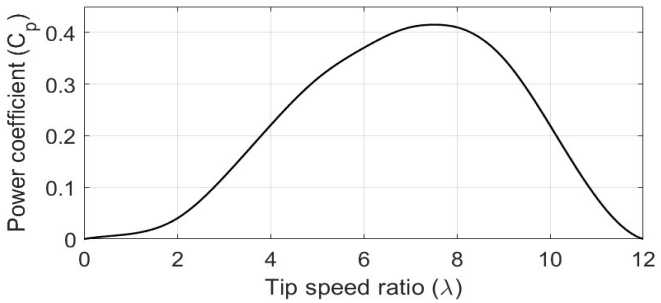

Figure 3. Power coefficient v/s tip speed ratio

FOREX Publication
Open Access | Rapid and quality publishing
International Journal of Electrical and Electronics Research (IJEER)
Research Article | Volume 14, Issue 2 | Pages 309-319 | e-ISSN: 2347-470X

The ideal expression of maximum power has been derived from substituting *equation (3)* into *(1)* as follows:

$$\begin{cases} P_{m-opt} & = \frac{1}{2}\rho\pi R^5 \omega_{m-opt}^3 C_{p-opt}/\lambda_{opt}^3 \\ P_{m-opt} & = K_{opt}\omega_{m-opt}^3 C_{p-opt} \end{cases} \quad (5)$$

where, ω_{m-opt} represents the ideal speed of rotation that corresponds to wind speed, and also K_{opt} denotes the power gain which is provided by

$$K_{opt} = \frac{1}{2}\rho\pi R^5 C_{p-opt}/\lambda_{opt}^3 \quad (6)$$

The MPPT control can be implemented using *equation (6)*.

2.3. Mathematical Model of DFIG

According to the circuit in *figure 4*, synchronous coordinates of the voltages are [24-26]:

$$\begin{cases} v_{ds} = R_s i_{ds} + \frac{d}{dt}\psi_{ds}(t) - w_s\psi_{qs} \\ v_{qs} = R_s I_{qs} + \frac{d}{dt}\psi_{qs}(t) + w_s\psi_{ds} \\ v_{dr} = R_r i_{dr} + \frac{d}{dt}\psi_{dr}(t) - w_r\psi_{qr} \\ v_{qr} = R_r i_{qr} + \frac{d}{dt}\psi_{qr}(t) + w_r\psi_{dr} \end{cases} \quad (7)$$

where, v_{ds}, v_{qs} denotes the stator voltages of *d-q* axis, v_{dr}, v_{qr} represents rotor voltages of *d-q* axis, ψ_{ds}, ψ_{qs} denotes stator fluxes of *d-q* axis , ψ_{dr}, ψ_{qr} denotes *d-q* axis rotor fluxes, i_{ds}, i_{qs} represents stator currents, i_{dr}, i_{qr} denotes rotor currents, R_s, R_r denotes stator as well as rotor resistances, w_s, w_r denotes ststor and rotor angular speeds.

The flux equations can be written as

$$\begin{cases} \psi_{ds} = L_s i_{ds} + L_m i_{dr} \\ \psi_{qs} = L_s i_{qs} + L_m i_{qr} \\ \psi_{dr} = L_r i_{dr} + L_m i_{ds} \\ \psi_{qr} = L_r i_{qr} + L_m i_{qs} \end{cases} \quad (8)$$

where, L_s denotes self-inductance of stator , L_r denotes self-inductance of the rotor, L_m denotes mutual inductance while σ denotes leakage factor given by

$$\sigma = (1 - \frac{L_m^2}{L_s L_r}) \quad (9)$$

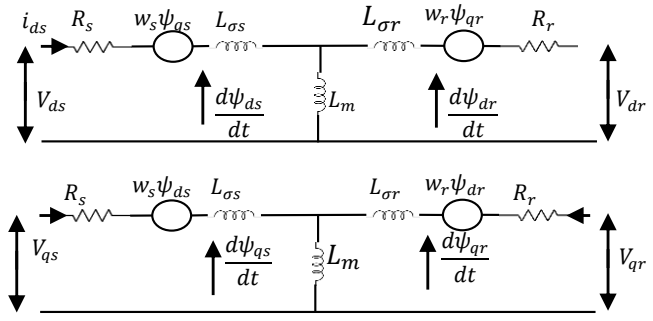

Figure 4. *d-q* Model of the DFIG in synchronous coordinates

3. CNTROL STRATEGY

3.1. Output Voltage Equation

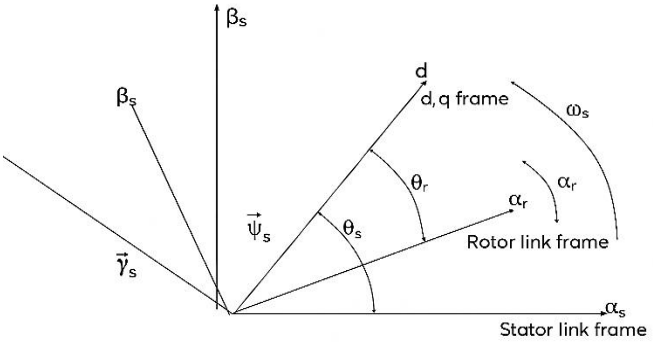

Figure 5. Vector diagram of stator flux-oriented control

The stator current components must be synchronized with the stator space vectors. This indicates that, as depicted in *figure 6*, the dq axes of the reference rotating frame are moving in front of one another [27].

Hence,

$$\begin{cases} \psi_{qs} & = 0 \\ \psi_{ds} & = \psi_s \end{cases} \quad (10)$$

Based on the previously stated equation, it is presumable that the system is stable, with voltage v_s leading the stator flux ψ_s. As *figure 6* illustrates, stator voltage can be simplified as follows:

$$\begin{cases} v_{ds} & = 0 \\ v_{qs} & = v_s = w_s\psi_s \end{cases} \quad (11)$$

Given that stator flux is directly proportional to voltage, the expression for stator flux in the steady state is obtained thus:

$$\begin{cases} \psi_{ds} = \psi_s & = L_s i_{ds} + L_m i_{dr} \\ 0 & = L_s i_{qs} + L_m i_{qr} \end{cases} \quad (12)$$

Therefore, the stator current equations can be obtained from the *equation (12)* as

$$\begin{cases} i_{ds} & = \frac{\psi_s}{L_s} - \frac{L_m}{L_s} i_{dr} \\ i_{qs} & = -\frac{L_m}{L_s} i_{qr} \end{cases} \quad (13)$$

The electromagnetic torque expression is given by

$$T_{em} = -\frac{3}{2}\rho\frac{L_m v_s}{L_s w_s} i_{qs} \quad (14)$$

4. MODEL REFERENCE ADAPTIVE CONTROLLER (MRAC)

MRAC uses technique of parameter estimation to minimize the output and the reference model' difference [28]. As seen in *figure 6*, the MRAC framework comprises three distinct components, wich are a reference model, the real plant, and an adaptive rule. One model, referred to as the uncertain dynamic system and is thought to be the original plant. Both uncertainity

FOREX Publication
Open Access | Rapid and quality publishing
International Journal of Electrical and Electronics Research (IJEER)
Research Article | Volume 14, Issue 2 | Pages 309-319 | e-ISSN: 2347-470X

model and the reference model receive the external input simultaneously. When output from reference model is compared to that of uncertain dynamic system, it represents the expected closed-loop dynamic system response and the error signal that the system produced powers the parameter modification procedure. The uncertain dynamical system's trajectories are then driven to match the reference model's trajectories by this method, which modifies the controller parameters.

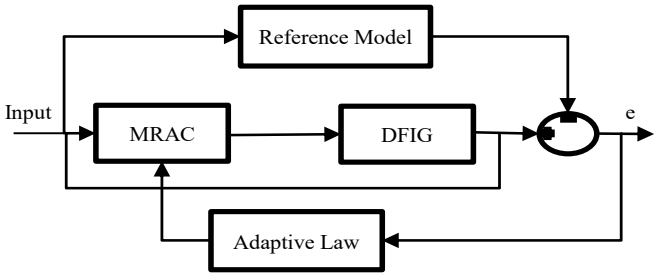

Figure 6. Schematic diagram of model reference adaptive controller

This work reports on the system of DFIG wind energy conversion; that is, State-Space form as given in Section [29].

$$\dot{x}(t) = Ax(t) + B[u(t) + \Delta x(t)]; x(0) = x_0 \quad (15)$$

In this case, a control vector is denoted by $u(t) \in \mathbb{R}^m$ and a measurable space vector is represented by $x(t) \in \mathbb{R}^n$. A known system matrix is indicated by the parameters $A \in \mathbb{R}^{n*n}$ and a known control matrix is indicated by $B \in \mathbb{R}^{n*m}$. Moreover, $\Delta: \mathbb{R}^n \to \mathbb{R}^m$ denotes an uncertainty of the system that is time-invariant.

Equation (15) requires the system uncertainty to be parameterized in order to implement model reference adaptive control. Depending on the type of system uncertainty $\Delta x(t)$, either structured or unstructured parametrizations can be considered. In this case, we assume that *equation (15)*'s system uncertainty satisfies the following structural representation.

$$\Delta x = W^T \beta(x); \ x \in \mathbb{R}^n \quad (16)$$

Where, $W \in \mathbb{R}^{s*m}$ denotes unidentified weight matrix and also $\beta: \mathbb{R}^n \to \mathbb{R}^s$ denotes basis function which is idenified.

In the proposed adaptive control formulation, the DFIG dynamics contain modeling uncertainties arising from parameter mismatch, grid disturbances, and unmodeled converter dynamics. These uncertainties include variations in stator and rotor resistances due to temperature, inductance deviations caused by magnetic saturation, and external disturbances introduced by wind speed fluctuation and grid voltage sag.

The uncertain term in *eq. (15)* is therefore represented as a structured parametric uncertainty of the form

$$\Delta(x,t) = W*^{\mathrm{T}} \varphi(x,t) \quad (17)$$

where W* denotes an unknown constant parameter matrix and φ(x,t) represents a known basis function vector derived from measurable states and inputs.

For practical implementation, the unknown parameter matrix is assumed to be bounded such that

$$\|W*\| \leq W_{max} \quad (18)$$

where W_{max} is a positive constant determined from machine parameter tolerance limits and expected operating variations.

In this work, parameter uncertainty bounds are selected within ±25% of nominal inductance and resistance values, which is consistent with variations reported in DFIG literature under thermal and magnetic operating conditions. This bounded representation allows formulation of a Lyapunov-based adaptive update law while ensuring stability under realistic parameter deviations.

In order to make the dynamic system state trajectory follow the state trajectory of reference model a state feedback control is considered as:

$$u(t) = u_n(t) - u_{ad}(t) \quad (19)$$

where $u_n(t)$ and $u_{ad}(t)$ are used respectively to designate the nominal control law and the adaptive control law. The former u_n(t) is such that:

$$\begin{cases} u_n(t) & = -K_1 x(t) + K_2 r(t) \\ u_{ad}(t) & = \widehat{W}^T(t)\beta(x(t)) \end{cases} \quad (20)$$

Where, $K_1 \in \mathbb{R}^{m*n}$ represents a matrix of feedback gain, and $K_2 \in \mathbb{R}^{m*n_r}$ stands for matrix of feedforward gain and $r(t) \in \mathbb{R}^{n_r}$ represents as a uniformly continuous bounded input command.

The reference model for the system has been chosen as:

$$\dot{x}_m(t) = A_m x(t) + B_m r(t) \quad (21)$$

Where, A_m and B_m are the reference model parameters. The nominal control law gain K_1 must be chosen in such that A_m is Hurwitz such that for a given $R > 0$, the Lyapunov equation $0 = A_m^T P + P A_m + I$ holds.

The dynamics of system errors is given below:

$$e(t) \stackrel{\Delta}{=} x(t) - x_m(t) \quad (22)$$

And the time derivative gives the following equations:

$$\begin{cases} \dot{e}(t) = \dot{x}(t) - \dot{x}_m(t) \\ \dot{e}(t) = A_m e(t) - B\widetilde{W}^T(t)\beta(x(t)) \end{cases} \quad (23)$$

The weight update law to drive the system error asymptotically to zero:

FOREX Publication
Open Access | Rapid and quality publishing
International Journal of Electrical and Electronics Research (IJEER)
Research Article | Volume 14, Issue 2 | Pages 309-319 | e-ISSN: 2347-470X

$$\begin{cases} \dot{\widehat{W}}(t) = & \Gamma f_{ad}(.);\ \Gamma > 0 \\ \dot{\widetilde{W}}(t) = & \dot{\widehat{W}} - \dot{W} \\ \dot{\widetilde{W}} = & \Gamma f_{ad}(.) \end{cases} \quad (24)$$

To verify that the control system designed is stable, we utilize the Lyapunov function candidate function in the form given by

$$V(e, \widetilde{W}) = e^T P e + \Gamma^{-1} tr \widetilde{W}^T \widetilde{W} \quad (25)$$

The Lyapunov function candidate's time derivative yields:

$$\begin{cases} \dot{V}(e, \widetilde{W}) = 2e^T(t) P \dot{e}(t) + 2\Gamma^{-1} tr \widetilde{W}^T \dot{\widetilde{W}} \\ \dot{V}(e, \widetilde{W}) = 2e^T(t) P A_m e(t) + 2e^T(t) \widetilde{W}^T(t) \\ \qquad [f_{ad}(.) - PBe^T \beta(x(t))] \end{cases} \quad (26)$$

If we choose our parameter adjustment mechanism as

$$\begin{cases} f_{ad}(.) \triangleq & \beta(x(t)) e^T(t) PB \\ \dot{\widehat{W}}(t) = & \Gamma \beta(x(t)) e^T(t) PB \end{cases} \quad (27)$$

which gives $\dot{V}(e, \widetilde{W}) = 2e^T(t) e(t) P A_m$.

Therefore, from Lyapunov equation we can write

$$\begin{cases} \dot{V}(e, \widetilde{W}) = & 2e^T(t) e(t) [P A_m^T + P A_m] \\ & = -e^T(t) e(t) I \end{cases} \quad (28)$$

It ensures Lyapunov stability for both estimate $\dot{\widehat{W}}(t)$ and system $e(t)$ errors.

Classical MRAC schemes may experience parameter drift when excitation conditions are insufficient or when disturbances persist for extended durations. To prevent unbounded growth of adaptive parameters, a projection-based update mechanism is incorporated into the adaptive law.

The modified weight update law is written as

$$\dot{W} = Proj(W, -\Gamma\, \varphi(x,t) e^T P\, B) \quad (29)$$

where Γ is a positive definite adaptation gain matrix and Proj(·) denotes a projection operator that constrains parameter estimates within predefined bounds.

The projection operator ensures that

$$\|\widehat{W}\| \leq W_{max} \quad (30)$$

thereby preventing parameter drift while maintaining Lyapunov stability.

In addition, a σ-modification term is introduced to improve robustness under disturbance and noise conditions. The modified adaptive law becomes

$$\dot{W} = -\Gamma\, \varphi(x,t) e^T P\, B - \sigma \widehat{W} \quad (31)$$

where σ is a small positive constant. This term introduces leakage in the adaptation mechanism and guarantees bounded parameter convergence even when persistent excitation conditions are weak.

4.1. Convergence Conditions and Persistent Excitation

The Lyapunov-based design guarantees boundedness of all closed-loop signals and asymptotic convergence of tracking error under standard MRAC assumptions. However, parameter convergence additionally requires a persistent excitation (PE) condition on the regressor vector φ(x,t).

The PE condition can be expressed as

$$\int t^{\{t+T\}} \varphi(\tau) \varphi^T(\tau) d\tau \geq \alpha I \quad (32)$$

for some positive constants α and T.

In wind energy systems, persistent excitation is naturally introduced by wind speed variations, grid disturbances, and power reference changes. The step and ramp wind profiles used in this study provide sufficient excitation for convergence of adaptive parameters.

Even in the absence of strict PE conditions, the projection-based and σ-modified adaptive law ensures bounded parameter estimates and stable tracking performance.

4.2. GSC Current Controller Design

In addition to controlling dc voltage, the GSC also manages reactive power. Utilizing the decoupled vector control technique, traditional GSC control strategy is implemented [10–15]. *Figure 7* shows the GSC's simplified circuit, with v_{a1}, v_{b1} and v_{c1} being the GSC voltages and, R and L corresponding series resistance and inductance filter, and, V_a, V_b and V_c are grid voltages [30,31].

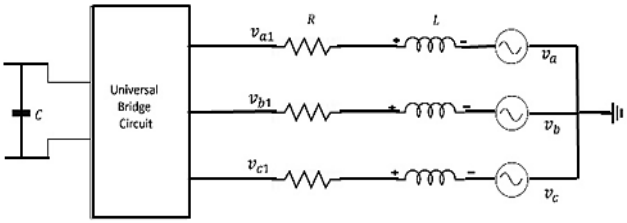

Figure 7. Grid-side converter circuit

The following equation can be obtained by using Kirchhoff voltage law and applying Park transformation in *figure 7*.

$$\begin{cases} v_{dg} = R i_{dg} + L \frac{di_{dg}}{dt} - \omega_s L i_{qg} + v_{d1} \\ v_{qg} = R i_{qg} + L \frac{di_{qg}}{dt} + \omega_s L i_{dg} + v_{q1} \end{cases} \quad (33)$$

Active and reactive powers, P_g and Q_g respectively, can be given as:

$$\begin{cases} P_g = \frac{3}{2}(v_{dg} i_{dg} + v_q i_{qg}) \\ Q_g = \frac{3}{2}(v_{qg} i_{dg} - v_d i_{qg}) \end{cases} \quad (34)$$

FOREX Publication
Open Access | Rapid and quality publishing
International Journal of Electrical and Electronics Research (IJEER)
Research Article | Volume 14, Issue 2 | Pages 309-319 | e-ISSN: 2347-470X

The coupling between the reactive and active powers is clearly seen by *equations (34)*. As a result, a vector-oriented technique has been used to decouple active & reactive powers ($v_{qg} = 0$; and $v_{dg} = constant$) which are expressed in the form of following equations:

$$\begin{cases} P_g = \frac{3}{2} v_{dg} i_{dg} \\ Q_g = \frac{3}{2} v_{dg} i_{qg} \end{cases} \quad (35)$$

Therefore, the grid voltages in synchronously rotating frame is:

$$\begin{cases} v_d &= Ri_{dg} + L\frac{di_{dg}}{dt} - \omega_s L i_{qg} + v_{d1}^* \\ 0 &= Ri_{qg} + L\frac{di_{qg}}{dt} + \omega_s L i_{dg} + v_{q1}^* \end{cases} \quad (36)$$

where, the reference voltages of the *d* as well as *q* axes are v_{d1}^*, v_{q1}^* respectively. Even so, there is an i_q, it is not contributing factor like a conventional close-loop control idea.

Thus, the current control loop is defined by the following equations:

$$\begin{cases} v_{d1}^* &= -Ri_{dg} - L\frac{di_{dg}}{dt} + \omega_s L i_{qg} + v_d \\ v_{q1}^* &= -Ri_{qg} - L\frac{di_{qg}}{dt} - \omega_s L i_{dg} \end{cases} \quad (37)$$

Where, the disturbances for both *d* and *q* axes are given as

$$D_{qd} = \pm\omega_s$$

Therefore, using *equations (36)* & *(37)*, the two voltage components across the inductor L can be adjusted to control both axis currents.

4.3. RSC Current Controller Design

To monitor the wind turbine's maximum power production characteristics and regulate machine behavior, the control approach used by converter on the machine side is more sophisticated. The machine side controller is consist of torque and reactive power control loop [30, 31]. By comparing the *dq*-axis current references to the actual currents of the inverter, the MRAC controller in the machine-side controller estimates the *dq*-axis voltages.

The rotor voltage is derived from the torque reference estimated by the observer.

$$\begin{cases} v_{dr} &= R_r i_{dr} + \sigma L_r \frac{d}{dt} i_{dr} - \omega_r \sigma L_r i_{qr} \\ v_{qr} &= R_r i_{qr} + \sigma L_r \frac{d}{dt} i_{qr} + \omega_r \sigma L_r i_{dr} + \omega_r \frac{{L_m}^2}{L_s} i_{dr} \end{cases} \quad (38)$$

Therefore, the state space model of *dq*-axis currents can be presented as:

$$\begin{cases} \frac{d}{dt} i_{dr} &= \frac{1}{\sigma L_r}[v_{dr} - R_r i_{dr} - \omega_r \sigma L_r i_{qr}] \\ \frac{d}{dt} i_{qr} &= \frac{1}{\sigma L_r}[v_{qr} - R_r i_{qr} - \omega_r \sigma L_r i_{dr} - \omega_r \frac{{L_m}^2}{L_s}] \end{cases} \quad (39)$$

Where, the disturbances for both *d* and *q* axes are given as

$$D_{dr} = -\omega_r$$

$$D_{qr} = \omega_r \frac{{L_m}^2}{L_s} + \omega_r \sigma L_r$$

4.4. DC Bus Voltage Controller Design

Voltage is written in terms of DC-link capacitor as power leaving GSC and entering grid from RSC. The MRAC technique for P_r is same as the method used for rotor current, which is injected into the rotor circuit, while the protocol for P_g is the same as the injected current into a grid [30, 31]:

$$C_{dc} V_{dc} \frac{dV_{dc}^2}{dt} = -P_r + P_g \quad (40)$$

Where, V_{dc}, P_r, P_g and C_{dc} are DC bus voltage, rotor active power, grid active power and dc-ink capacitor respectively.

From *equation (34)* and assuming small DC bus voltage variation, we have

$$C_{dc} V_{dc} \frac{d}{dt} V_{dc} = -P_r + v_d i_d \quad (41)$$

Therefore, it is possible to adjust the axis currents by controlling the DC bus voltage.

4.5. Simulation Environment and Numerical Configuration

The proposed MRAC-based DFIG control strategy was validated using MATLAB/Simulink environment to evaluate dynamic and steady-state performance under controlled operating conditions. The simulation model includes detailed representations of the wind turbine, DFIG electrical dynamics, back-to-back converters, DC-link capacitor, grid interface filter, and control subsystems.

The simulations were executed using a discrete solver to accurately capture switching dynamics and controller adaptation behavior. Key simulation parameters are summarized in *table 1*.

Table 1. Simulation Configuration Parameters

Parameter	Value
Simulation platform	MATLAB/Simulink
Solver type	Discrete (ode3 / fixed-step)
Simulation step size	5 µs
Control sampling time	50 µs
PWM switching frequency	5 kHz
Simulation duration	10 s
Grid frequency	50 Hz
Converter model	IGBT-based PWM VSI
Numerical method	Forward Euler discretization

A fixed-step discrete solver was selected to emulate real-time digital controller implementation and to ensure numerical stability of the adaptive update law. The sampling period was chosen sufficiently smaller than converter switching dynamics to avoid discretization-induced instability.

FOREX Publication
Open Access | Rapid and quality publishing
International Journal of Electrical and Electronics Research (IJEER)
Research Article | Volume 14, Issue 2 | Pages 309-319 | e-ISSN: 2347-470X

5. SIMULATION RESULTS AND DISCUSSION

MATLAB/Simulink-based validation represents a widely accepted first-stage verification approach for advanced control algorithms in wind energy systems, allowing controlled evaluation of nonlinear dynamics, parameter uncertainties, and disturbance scenarios prior to experimental deployment. The developed model incorporates switching converters and grid interaction dynamics, enabling realistic assessment of controller performance.

The objective of this study is to establish theoretical stability and control effectiveness of the proposed MRAC framework. Hardware implementation and experimental verification are considered future extensions following controller parameter tuning and safety validation.

Evaluation for effectiveness of suggested control strategy with a VC methodology is examined in this section through simulation on a 2 MW WECS wich is based on DFIG using MATLAB/Simulink under various operating scenarios. The simulation datas are given in *table 2* and *table 3*. The maximum wind power is tracked using the MPPT algorithm. The system performance can be summarized under different conditions using current control loop.

Table 2. DFIG and Wind Turbine Parameters

Parameter	Description	Value
N	Synchronous speed	1800 rpm
R_w	Rotor blade radius	42 m
C_{bus}	Bus capacitor	8×10^3 F
J	System inertia	100 $k_g.m^2$
G	Gearbox ratio	100
C_p	Turbine power coefficient	$C\_1 = 0.5109, C\_2 = 116, C\_3 = 0.04, C\_4 = 5, C\_5 = 21, C\_6 = 0.0068$
P_{rated}	DFIG rated power	$2MW$
p	Pole pair number	2
I_{s_rated}	Stator rated current	1760 A
R_s	Stator resistance	2.6 $m\Omega$
L_s	Stator self-inductance	2.6 mH
L_m	Mutual inductance	2.5 mH
R_r	Rotor resistance	2.9 $m\Omega$
L_r	Rotor self-inductance	2.6 mH

Table 3. Grid Parameters

Parameter	Description	Value
V_s	Line-to-line grid voltage	690 V
f	Grid frequency	60 Hz
C_{bus}	Bus capacitor	8×10^3 F
R_g	Grid filter resistance	20×10^{-6}H
L_g	Grid filter inductance	483×10^{-6}H
V_{dc}	DC bus voltage reference	1200 V

In *figure 8*, the system simulink model is shown. *Figure 9* shows that repeated step is changing in the wind speed.

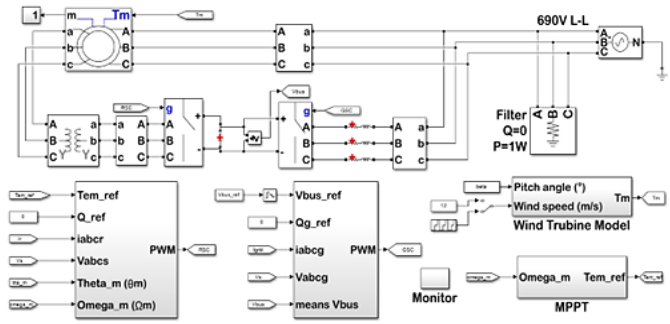

Figure 8. Simulink Model of DFIG

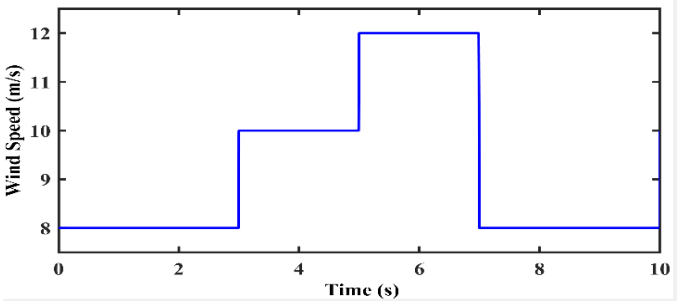

Figure 9. Wind Speed in Step Response

Step changes in wind speed (8 m/s, 10 m/s, and 12 m/s) are applied to evaluate system performance under sub-synchronous and super-synchronous operating modes as presented in *figure 8 & 9* displays the machine side performance with MRAC under wind speed variations in step changes. The rotor speeds as illustrated in *figure 10(a)* is as follows: 1486 rpm at 8 m/s wind speeds, 1880 rpm at 10 m/s wind speeds, and 2267 rpm at 12 m/s wind speeds.

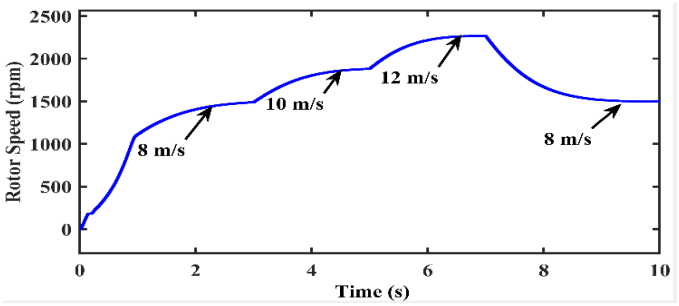

(a)

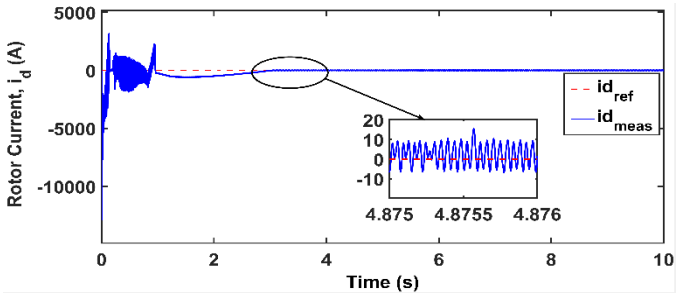

(b)

FOREX Publication
Open Access | Rapid and quality publishing
International Journal of Electrical and Electronics Research (IJEER)
Research Article | Volume 14, Issue 2 | Pages 309-319 | e-ISSN: 2347-470X

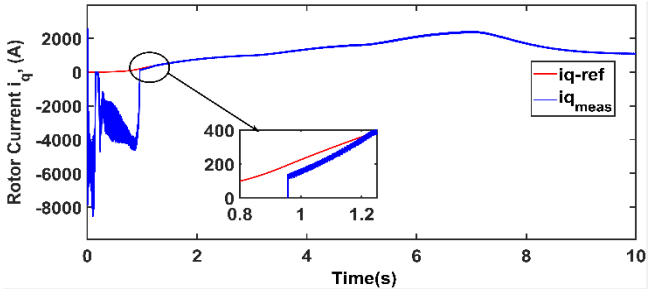

(c)

Figure 10. Current control loop of RSC with MRAC

At all wind speeds, the rotor keeps its ideal speed. *Figure 10(b)* & *figure 10(c)* illustrate response of the control loops using MRAC. The reference currents *iq* taken from the MPPT are exactly followed by the rotor currents without any overshoot, as the graphs demonstrate.

The response of control loops on GSC using MRACis presented in *figure 11*. The GSC side current *id* is displayed in *figure 11(a)* DC bus voltage scope is displayed in *figure 11(b)*.

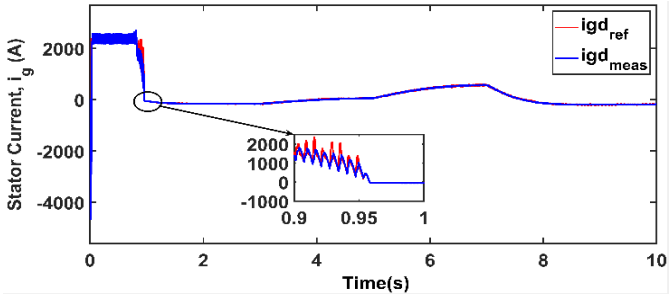

(a)

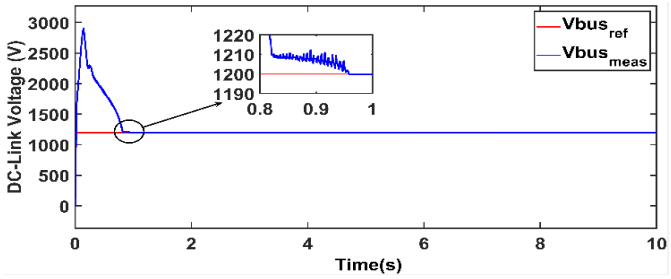

(b)

Figure 11. Scope of control loop for GSC with MRAC

It is seen from the figures that the grid current id smoothly tracks the reference current. The grid-side converter maintains stable DC-link voltage regulation throughout operation despite wind speed variation, demonstrating effective decoupling between active and reactive power control loops.

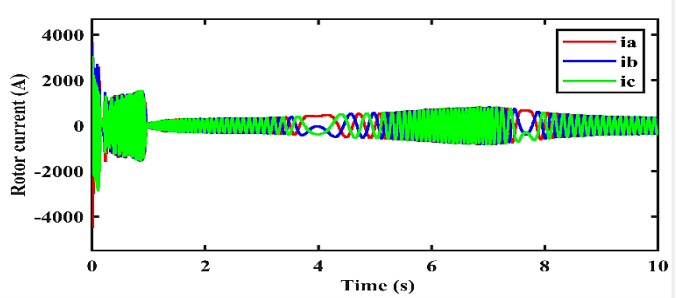

(a)

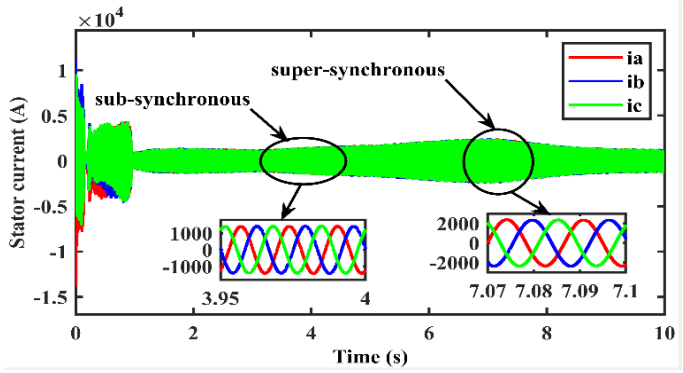

(b)

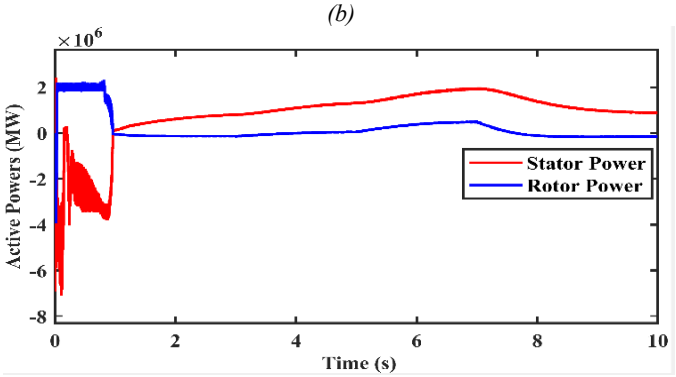

(c)

Figure 12. Current and power response to speed change

The power generations and the phase currents presented in figure 12 (all) while the phase current of rotor in *figure 12(a)*, the stator phase current is represented by *figure 12(b)* & *figure 12(c)* displays the rotor and stator active powers. *Figure 12 (a)* shows how the frequency of rotor current shifts sub-synchronous mode to highly synchronous mode through the synchronous speed. Both stator and rotor powers generations presented in *figure 12(c)*. demonstrate the mode of operations.

5.1. Comparative simulation with conventional PI or other methods

A comparison study was suggested between the proposed MRAC strategy versus a conventional PI-based vector control system under identical wind profiles. *Figure 13* compares the DC-link voltage, rotor speed, and current response of both methods. It is observed from the *table 3*, that while PI controller shows sluggish response with minor overshoot (~9%), the MRAC-based system achieves <5% overshoot with quicker settling.

Table 4. Presents Detailed Comparison

Metric	PI Control	Proposed MRAC
DC-Link Overshoot (%)	9.1%	4.3%
Settling Time (s)	0.47	0.31
Steady-State Error (A)	0.12	~0.01
Rotor Speed Tracking Error	High	Low

FOREX Publication
Open Access | Rapid and quality publishing
International Journal of Electrical and Electronics Research (IJEER)
Research Article | Volume 14, Issue 2 | Pages 309-319 | e-ISSN: 2347-470X

These results confirm the outstanding tracking performance and dynamic robustness of the MRAC schemes. *Figure 13*, simulated comparison of DC-link voltage and rotor speed response under step wind speed input. The MRAC settles faster with less overshoot and offers better tracking performance than the classical PI controller.

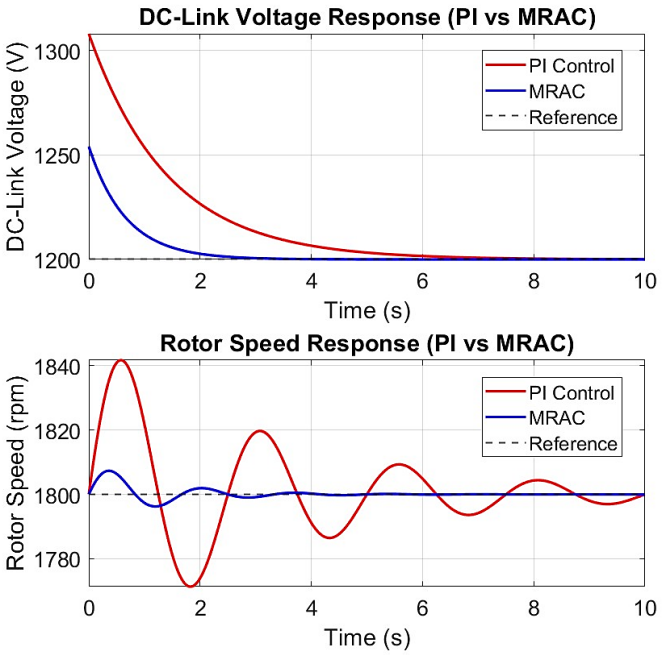

Figure 13. Comparative Response of PI and MRAC Controllers

5.2. Robustness Under Disturbance and Fault Scenarios

The robustness of the proposed MRAC control scheme was tested under three disturbance types: a 3-phase short-circuit fault for 100ms; inductance variation faults of ±25%; and grid voltage sag to 0.7 per unit. In the wake of such disturbances, the MRAC managed to keep the DC-link voltage from deviating more than 7% from its nominal value and rapidly restored active and reactive powers. Rotor speed activity remained good with minimal oscillations. The system settles very fast at around 0.2 seconds after fault clearance. This response confirms the strong disturbance rejection capability and adaptive robustness of the proposed MRAC framework under grid-connected fault conditions.

A ±25% parameter variation in inductance and resistance was introduced to validate bounded-uncertainty assumptions used in the MRAC design.

To provide systematic performance assessment, quantitative metrics were extracted from simulation responses under disturbance scenarios including grid voltage sag, parameter variation, and short-circuit fault conditions. The following indices were evaluated:

- Maximum overshoot (%)
- Settling time (s)
- Steady-state error
- DC-link voltage deviation (%)
- Power recovery time (s)

Table 5. Quantitative robustness performance under disturbances

Disturbance Scenario	Overshoot (%)	Settling Time (s)	DC-Link Deviation (%)	Power Recovery Time (s)
Wind speed step	4.3	0.31	3.8	0.35
Grid voltage sag (0.7 pu)	6.2	0.28	6.5	0.32
±25% parameter variation	4.8	0.30	5.1	0.34
3-phase fault (100 ms)	6.9	0.22	7.0	0.27

The results demonstrate that the adaptive controller maintains bounded response and rapid recovery across all disturbances, confirming robustness of the MRAC strategy under realistic operating uncertainties.

5.3. Comparative Evaluation with Advanced Nonlinear Controllers

Although the proposed control strategy is compared in detail with a conventional PI-based vector controller, it is also important to position the developed MRAC framework with respect to other advanced nonlinear control approaches that have been reported for DFIG-based wind energy systems. Several studies have investigated sliding mode control (SMC), model predictive control (MPC), and artificial intelligence-based controllers for improving robustness and dynamic performance of DFIG systems. A qualitative benchmarking of these controllers with the proposed MRAC scheme is therefore presented in *table 4* based on reported performance metrics in recent literature.

Table 6. Qualitative Comparison of Control Strategies for DFIG-Based WECS

Controller	Computational Complexity	Robustness to Parameter Variation	Sensor Requiremen	Typical Overshoot
PI Control	Low	Low	Low	~9%
Proposed MRAC	Medium	High	Low	4.3%
Sliding Mode Control (SMC)	High	Very High	Medium	~3–5%
Model Predictive Control (MPC)	Very High	High	High	~2–4%

The classical PI controller is simple and widely used in industrial wind turbine systems. However, its fixed-gain structure makes it sensitive to parameter uncertainties and wind fluctuations, which leads to slower transient response and larger overshoot. In contrast, the proposed MRAC scheme adapts controller parameters online using a Lyapunov-based update law, which improves tracking accuracy and disturbance rejection capability without requiring gain retuning.

Sliding mode control has been reported to provide strong robustness against disturbances and parameter variation.

FOREX Publication
Open Access | Rapid and quality publishing
International Journal of Electrical and Electronics Research (IJEER)
Research Article | Volume 14, Issue 2 | Pages 309-319 | e-ISSN: 2347-470X

However, the discontinuous switching action introduces chattering, which can cause additional stress on power electronic converters and increase harmonic distortion. Implementation of SMC also requires careful boundary layer design and higher sampling rates.

Model predictive control provides excellent transient response and constraint handling capability. Nevertheless, MPC requires an accurate plant model and involves repeated online optimization, which significantly increases computational burden. Real-time implementation of MPC for high-frequency converter control typically demands powerful processors or FPGA-based platforms.

Compared with these advanced controllers, the MRAC scheme proposed in this work offers a balanced trade-off between robustness, computational complexity, and implementation feasibility. The controller relies only on standard *dq*-axis voltage and current measurements and does not require complex optimization routines or high-frequency switching logic. Unlike neural network-based approaches, the proposed method does not involve training procedures or large data requirements. The adaptive law ensures convergence of tracking error while maintaining a computational structure that can be implemented on conventional DSP-based wind turbine controllers.

Therefore, while MPC and SMC may achieve slightly lower overshoot under certain conditions, the proposed MRAC strategy provides competitive dynamic performance with significantly lower implementation complexity and improved practical feasibility for grid-connected wind energy systems.

5.4. Feasibility and Implementation Aspects

The proposed MRAC scheme is suitable for real-time deployment using low-cost Digital Signal Processors (DSPs) or FPGAs due to its recursive parameter update structure and lack of complex observer-based estimations. Unlike predictive control methods, MRAC has reduced computational complexity. Its reliance only on standard *d-q* quantities (voltages/currents) makes it practical with existing sensor infrastructure. The algorithm can be implemented using standard lookup tables and integration blocks on embedded platforms (e.g., TI TMS320 series).

In practical digital implementation, measurement noise, discretization effects, and sensor imperfections can influence adaptive controller performance. The *dq*-axis voltages and currents used in the MRAC scheme are obtained through standard sensors and phase-locked loop estimation, which introduces quantization and filtering delays. To mitigate noise amplification in the adaptive loop, the regressor vector is filtered using a first-order low-pass filter before parameter update.

The adaptive law is discretized using a forward Euler method with sampling time of 50–100 μs, which is consistent with converter switching frequency. Stability of the discretized adaptive system is maintained by selecting adaptation gain Γ within bounds determined through simulation.

Sensor offset and noise effects are further reduced by normalizing current and voltage measurements in per-unit form. These implementation considerations ensure that the proposed MRAC strategy remains stable and realizable on DSP or FPGA-based wind turbine control platforms.

Although experimental validation is beyond the scope of the present study, the proposed controller architecture is designed to be compatible with real-time implementation platforms. The adaptive algorithm requires only algebraic parameter updates and avoids computationally intensive optimization routines, making it suitable for DSP or FPGA realization.

Hardware-in-the-Loop (HIL) validation can be conducted using real-time simulators such as OPAL-RT or dSPACE platforms, where the power stage is emulated while the controller operates on embedded hardware. The discrete-time implementation adopted in this work directly supports such deployment without structural modification.

Future work will focus on real-time HIL validation to evaluate latency effects, measurement noise, and converter nonlinearities under practical operating conditions.

5.5. Potential Deployment Challenges

Some of the key challenges in implementing the MRAC strategy are sensitivity issues caused by initialization errors, parameter drift with time, and adaptation speed limitations on very nonlinear or fast grid conditions. In this regard, one way in which bounded adaptation laws or projection algorithms can be employed is to prevent parameter drift and guarantee stability, while another way in which MRAC can be combined with PI or Sliding Mode controllers during plant startup transients by means of which provided robustness is improved. Real-time parameter estimation under safe bounds may also significantly enhance the reliability of control approaches. Experimental validations with hardware-in-the-loop (HIL) simulation platforms are also suggested before proceeding with a grid-connected experiment to evaluate dynamic behavior and perform more accurate fine-tuning of adaptation mechanisms in realistic scenarios.

6. CONCLUSION

This paper attempts to present a robust Model Reference Adaptive Control (MRAC) based control strategy for power regulation of DFIG WECS. The MRAC scheme is merged with a vector-oriented control for the RSC and GSC to realize very close tracking of the reference currents and voltage regulation under varying wind conditions. Unlike existing control schemes using the PI or fixed-parameter controllers, with the MRAC scheme the parameters of the controller are adapted dynamically to offer better performance in nonlinear and uncertain environments. Hence, no repeated gain tuning or integration of other extensive sensors are needed. Using a Lyapunov-based adaptive law, global asymptotic stability is ensured with guaranteed convergence of the control error, which has been verified by simulation results. The novelty is in the design of an MRAC combined with flux-oriented control applied to both machine- and grid-side converters, thereby realizing an effective decoupled-control scheme without any additional observer model or speed sensors. The MRAC-based system achieved less than 5% DC-link voltage overshoot, rapid transient response, and complete power decoupling across wide

FOREX Publication
Open Access | Rapid and quality publishing
International Journal of Electrical and Electronics Research (IJEER)
Research Article | Volume 14, Issue 2 | Pages 309-319 | e-ISSN: 2347-470X

wind speed variations. Compared to previous literature, that generally focuses on classical vector control, PI-based MRAS observers, or fuzzy schemes, this work shows superior performance in terms of stability, adaptability, and minimal overshoot. Therefore, the proposed strategy provides an effective, scalable solution for smart wind power systems requiring minimal human intervention and high reliability.

Detailed simulation configuration and quantitative robustness metrics have been provided to ensure reproducibility and systematic validation of controller performance.

A qualitative benchmarking with advanced nonlinear controllers such as sliding mode control and model predictive control further confirms that the proposed MRAC strategy achieves a favorable trade-off between robustness, implementation complexity, and dynamic performance for practical wind energy applications.

REFERENCES

[1] Pena, Ruben, J. C. Clare, and G. M. Asher. "Doubly fed induction generator using back-to-back PWM converters and its application to variable-speed wind-energy generation." IEE Proceedings-Electric power applications 143.3 (1996): 231-241. 2(5), 99–110 (2016).

[2] Datta, Rajib, and V. T. Ranganathan. "A simple position-sensorless algorithm for rotor-side field-oriented control of wound-rotor induction machine." IEEE Transactions on Industrial Electronics 48.4 (2001): 786-793.

[3] Lajimi, A. Babaie, S. Asghar Gholamian, and M. Shahabi. "Modeling and control of a DFIG-based wind turbine during a grid voltage drop." Engineering, Technology & Applied Science Research 1.5 (2011): 121-125.

[4] Xu, Longya, and Wei Cheng. "Torque and reactive power control of a doubly fed induction machine by position sensorless scheme." IEEE transactions on Industry Applications 31.3 (1995): 636-642.

[5] S. A., and J. L. R. Amenedo. "Grid synchronisation of doubly fed induction generators using direct torque control." IEEE 2002 28th Annual Conference of the Industrial Electronics Society. IECON 02. Vol. 4. IEEE, 2002.

[6] Bogalecka, E. "Power control of a double fed induction generator without speed or position sensor." 1993 Fifth European Conference on Power Electronics and Applications. IET, 1993.

[7] Noguchi, Toshihiko, et al. "Direct power control of PWM converter without power-source voltage sensors." IEEE transactions on industry applications 34.3 (1998): 473-479.

[8] Datta, Rajib, and V. T. Ranganathan. "Direct power control of grid-connected wound rotor induction machine without rotor position sensors." IEEE Transactions on Power Electronics 16.3 (2001): 390-399.

[9] Xu, Lie, and Phillip Cartwright. "Direct active and reactive power control of DFIG for wind energy generation." IEEE Transactions on energy conversion 21.3 (2006): 750-758.

[10] hi, Dawei, Lie Xu, and Barry W. Williams. "Model-based predictive direct power control of doubly fed induction generators." IEEE Transactions on Power Electronics 25.2 (2009): 341-351.

[11] Zhang, Yongchang, et al. "A simple method to reduce torque ripple in direct torque-controlled permanent-magnet synchronous motor by using vectors with variable amplitude and angle." IEEE Transactions on Industrial Electronics 58.7 (2010): 2848-2859.

[12] Y. Zhang and J. Zhu, "Direct torque control of permanent magnet synchronous motor with reduced torque ripple and commutation frequency," IEEE Transactions on Power Electronics" vol. 26, no. 1, pp. 235- 248, 2011.

[13] Marques, G. D., et al. "A DFIG sensorless rotor-position detector based on a hysteresis controller." IEEE Transactions on Energy Conversion 26.1 (2010): 9-17.

[14] Pena, Ruben, et al. "Sensorless control of doubly-fed induction generators using a rotor-current-based MRAS observer." IEEE Transactions on Industrial electronics 55.1 (2008): 330-339.

[15] Cardenas, R., et al. "Sensorless control of a doubly-fed induction generator for stand alone operation." 2004 IEEE 35th Annual Power Electronics Specialists Conference (IEEE Cat. No. 04CH37551). Vol. 5. IEEE, 2004.

[16] Cardenas, R., et al. "MRAS observer for doubly fed induction machines." IEEE transactions on energy conversion 19.2 (2004): 467-468.

[17] Lu, Lin-Yu, et al. "Model reference adaptive back-electromotive-force estimators for sensorless control of grid-connected DFIGs." IEEE Transactions on Industry Applications 54.2 (2017): 1701-1711.

[18] Das, Ranjay. "Estimation of rotor position of a sensorless doubly fed induction generator." ADBU Journal of Engineering Technology 10.3 (2021).

[19] Abdallah, M. E., Arafa, O. M., Shaltot, A., & Abdel-Aziz, G. A. (2016, December). MRAC-based vector oriented control of a wind turbine-driven DFIG. In 2016 Eighteenth International Middle East Power Systems Conference (MEPCON) (pp. 597-603). IEEE.

[20] Djebbri, Sihem, Hanane Balaska, and Samir Ladaci. "Robust MRAC-based adaptive control of a Doubly Fed Induction Generator (DFIG) in a Wind energy system using a fractional order Integrator." Algerian Journal of Signals and Systems 5.1 (2020): 40-46.

[21] Yang, Bo, et al. "Nonlinear maximum power point tracking control and modal analysis of DFIG based wind turbine." International Journal of Electrical Power & Energy Systems 74 (2016): 429-436.

[22] Chojaa, Hamid, Aziz Derouich, Mohammed Taoussi, Seif Eddine Chehaidia, Othmane Zamzoum, Mohamed I. Mosaad, Ayman Alhejji, and Mourad Yessef. "Nonlinear control strategies for enhancing the performance of DFIG-based WECS under a real wind profile." *Energies* 15, no. 18 (2022): 6650.

[23] Liu, Jizhen, et al. "A novel MPPT method for enhancing energy conversion efficiency taking power smoothing into account." Energy Conversion and Management 101 (2015): 738-748.

[24] Chojaa, H., Derouich, A., Chehaidia, S. E., Zamzoum, O., Taoussi, M., & Elouatouat, H. (2021). Integral sliding mode control for DFIG based WECS with MPPT based on artificial neural network under a real wind profile. Energy Reports, 7, 4809-4824.

[25] Yonis, S. A., Yusupov, Z., Habbal, A., & Toirov, O. (2023). Control approach of a grid connected DFIG based wind turbine using MPPT and PI controller. Advances in Electrical and Electronic Engineering, 21(3), 157-170.

[26] Achar, A., Djeriri, Y., Benbouhenni, H., Bouddou, R., & Elbarbary, Z. M. S. (2024). Modified vector-controlled DFIG wind energy system using robust model predictive rotor current control. Arabian Journal for Science and Engineering, 1-25.

[27] G. S. Kaloi, J. Wang and M. H. Baloch, "Active and reactive power control of the doubly fed induction generator based on wind energy conversion system," Energy Reports 2, pp. 194-200, 2016.

[28] Zhang, Dan, and Bin Wei. "A review on model reference adaptive control of robotic manipulators." Annual Reviews in Control 43 (2017): 188-198.

[29] Yucelen, Tansel. "Model reference adaptive control." Wiley Encyclopedia of Electrical and Electronics Engineering (1999): 1-13.

[30] Singh, Pradeep, Krishan Arora, and Umesh C. Rathore. "Control strategies for improvement of power quality in grid connected variable speed WECS with DFIG–An overview." In Journal of Physics: Conference Series, vol. 2327, no. 1, p. 012008. IOP Publishing, 2022.

[31] Chojaa, Hamid, Aziz Derouich, Othmane Zamzoum, Said Mahfoud, Mohammed Taoussi, Hani Albalawi, Habib Benbouhenni, and Mohamed I. Mosaad. "A novel DPC approach for DFIG-based variable speed wind power systems using DSpace." IEEE Access 11 (2023): 9493-9510.